SPHEREx Target List of Ices Sources (SPLICES) Release Notes

Version: 8.6, 2024/11/20

Authors: Matthew Ashby, Joseph Hora, Volker Tolls, Miju Kang, Jeong-Eun Lee, Kyla Noh, and the *SPHEREx* Ices Team

Contents

Revision History

Table 1: Revision History

Version	Date	Comments
8.6	2024/11/20	SPLICES version 8.6: Added proximity analysis results,
		evaluation of relative position of sources for the Zucker et al. (2020)
		list of star forming region distances, standard stars, number of clouds
		along the line of sight analysis, and WISE short-term variability analysis.
7.3	2023/04/28	Removed duplicate sources and bright source artifacts.
7.2	2023/04/19	WISE W1 and W2-only sources added.

1   Introduction

Version 7.1 of the SPHEREx Target List of Ice Sources (SPLICES) is fully described in Ashby et al. (2023). This document describes subsequent updates to SPLICES, of which the latest is version 8.6. This version contains 9.9×10^6 targets, many of which are thought likely to present infrared absorption features due to water ice and other volatile species in the solid (ice) phase.

2   Version 7.2

The two main color-based target selection criteria used to compile SPLICES rely on the relatively shallow 2MASS PSC. This means they have a built-in shortcoming, in that they will tend to be biased against $JHKs$-faint sources. In other words, both of the two main target selections might miss the most deeply embedded objects, as well as sources situated behind the thickest screens of obscuring dust, because emission from such objects, even if detected by WISE, might be too attenuated to appear in the 2MASS PSC. To mitigate this bias we supplemented SPLICES with a WISE-only selection intended to identify more highly obscured objects. The selection criteria are quantified below.

WISE-only targets were required to be well-detected in both short-wavelength WISE bands in order to be included. Specifically, they had to be brighter than $W1 = 14.7$ and $W2 = 13.3$ mag. The AllWISE photometric quality flags for both $W1$ and $W2$ were required to be "A". Furthermore, to select for obscured sources, the colors were required to be red, such that $W1 - W2 > 0.1$.

To ensure spectral purity in the eventual SPHEREx spectra, sources satisfying the above brightness and color criteria were rejected if the AllWISE flag n2MASS was anything other than 0 or 1 (to reject sources with multiple close neighbors). Sources were also rejected if they had more than one 2MASS PSC source within $6\rlap{.}''2$. At this stage, duplications of prior SPLICES targets were also rejected.

As an additional check, the spatial distribution of sources satisfying the above constraints which were also detected in 2MASS was then examined. Those with near-IR colors $(J - K) < 0.45(H - W2) + 1.2$ and $(J - K) > 2.5(H - W2) + 0.1$ were removed from the list, because they seemed to be distributed uniformly over the sky, whereas objects not satisfying these two criteria were associated with dark clouds.

A final step was performed 'by hand' to remove spurious objects around bright WISE sources. This was necessary because the $W1 - W2 > 0.1$ color criterion selects spurious peaks in the WISE diffraction spikes. We therefore removed sources that were flagged as possible diffraction pattern objects in the WISE catalog. We also performed a visual search for other spurious objects by inspecting the nearby fields around bright WISE sources ($W1 < 4$ mag) and removing artifacts forming obvious large-scale cross or circle patterns.

The roughly 278,000 objects satisfying all the WISE-only selection criteria described above are flagged as `W1mW2` in the `SEL_TYPE` column of SPLICES.

3   Version 7.3

To make SPLICES version 7.3, a small number of duplicate sources (those found to have the same "designation" keyword) were identified and removed from SPLICES version 7.2. Also, a small number of spurious AllWISE-only detected sources that had been added to SPLICES version 7.2 were removed by hand, because these were found to correspond to the diffraction spikes around bright stars.

4   Version 8.6

A total of 1,015,790 new targets were added to SPLICES since version 7.3, bringing the total number of sources to 9,925,600. Additional columns were also added for a total of 151 columns in this version, with the full list shown in Table 3. The following subsections describe the major additions and changes.

4.1   SPHEREx Reference Catalog ID

The column `source_id` has been changed to be the unique long integer source ID from the SPHEREx reference catalog, which is the full list of sources for which the SPHEREx L1-3 pipeline will photometer and

produce spectra. This identifier is used to correlate sources in the SPLICES list to the L3 pipeline products which will include the native photometry for each source.

The `designation` column is a second way to refer to the source, and is more human-readable since it is in general the WISE source designation constructed from the right ascension and declination of the source in the WISE allsky catalog. Note that this may differ from the values in the `ra` and `dec` columns because these were taken from the Gaia or 2MASS positions, if detected in those surveys.

4.2   Av Estimate

Estimates of the total visual extinction (Av) of the SPLICES targets have been added (column `Av`). The value is based on the $H-W2$ color, or if no H-band measurement is available, the $K-W2$ color, as described in Ashby et al. (2023) based on the Rayleigh-Jeans Color Excess Method (Majewski et al., 2011). If no H or K magnitude is available, this column is left blank.

Note that the Av estimate is valid only for main sequence stars over a range of temperatures (Majewski et al., 2011), and it therefore will not be valid for objects such as YSOs and other intrinsically red objects like asymptotic giant branch (AGB) stars.

4.3   Machine Learning Source Classification

The final machine learning (ML) classification results were added to the columns previously defined for those items (`STYPE_ML, STYPE_ML_PROB1, STYPE_ML_PROB2`) as described in Ashby et al. (2023) and Lakshmipathaiah et al. (2023). The classes in `STYPE_ML` include AGN (active galactic nucleus), C AGB (carbon-rich AGB star), O AGB (oxygen-rich AGB star), Class I YSO (young stellar object), Class II YSO, Class III YSO, Flat spectrum YSO, and MS Star (main sequence star).

4.4   Low-Av Sources

A set of low-Av (<2 mag) sources were added in order to be able to accurately determine the minimum Av where ices begin to form on dust grains in the ISM, and to obtain a sample of relatively unobscured stars along lines of sight towards nearby molecular clouds to characterize the foreground dust absorption. Several regions were chosen based on the distances and regions of the sky defined in Zucker et al. (2020). Regions several degrees away from the Galactic plane were chosen towards well-studied nearby clouds in order to minimize the total number of sources being added to SPLICES. All sources in the selected regions that were not already included in SPLICES and satisfied the same isolation and minimum brightness criteria were added, for a total of 826,638 new targets. These are designated in the catalog by `SEL_TYPE = LOW_AV`. The sky distribution of the low-Av sources is shown in Figure 1.
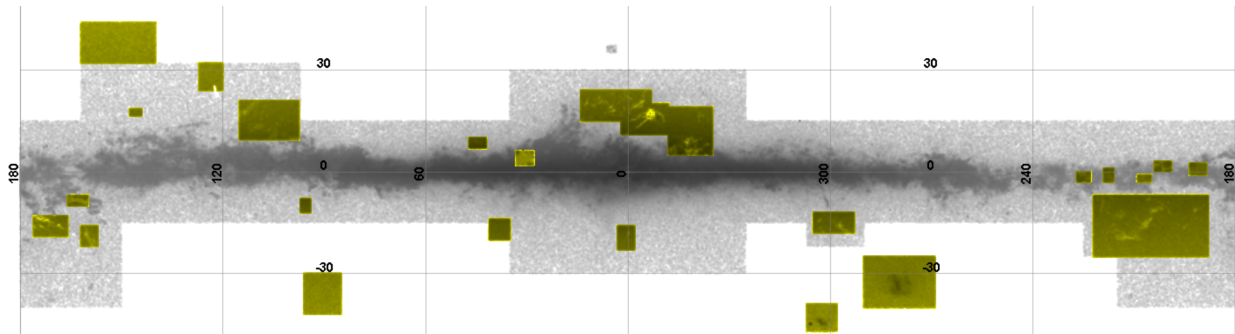

Figure 1: Location of the low-Av (color points) sources added to SPLICES version 8.6, shown against the SPLICES version 7.3 sources (gray). The plot is in Galactic coordinates.

4.5   Debris Disk Candidates

A set of debris disk candidate stars were added to version 8.6 of SPLICES. The objects were taken from lists published by Chen et al. (2014), Patel et al. (2014), Mittal et al. (2015), and Patel et al. (2017). A total 495 sources in these lists satisfied the SPHEREx isolation and minimum brightness criteria, and were added to SPLICES. They are indicated with SEL_TYPE = DEBRIS.

4.6   LAMOST and ATLAS standard stars

A number of photometric standard stars were added to SPLICES so that they will be processed in the same way as the SPHEREx science targets. The LAMOST and ATLAS standards provide examples of relatively unobscured and well-characterized stellar spectra to validate spectral fitting routines with the SPHEREx spectrophotometry, in a regime free from ice absorption features. Specifically, the stars added to SPLICES include lists from LAMOST and ATLAS-A, which are described in more detail below. The sky distribution of the standard stars is shown in Figure 2.
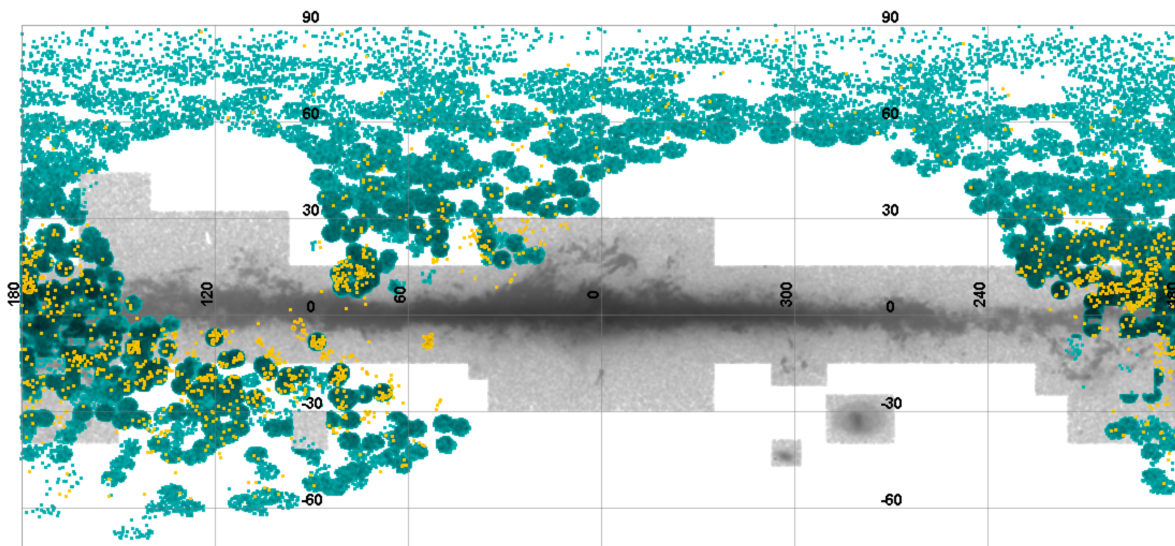

Figure 2: Location of the ATLAS (yellow points) and the LAMOST (green points) standard stars, shown against the SPLICES v. 7.3 sources (gray). The plot is in Galactic coordinates.

4.6.1   ATLAS Standards

The LAMOST survey (Cui et al., 2012) uses a 4 m reflective Schmidt telescope with 4000 fibers on a 20 square degree focal plane to obtain R~1800 spectra in the optical wavelength range 3700–8700 Å. The recently published ATLAS-A library (Ji et al., 2023) provides a homogeneous set of stellar spectra with good absolute-flux calibration. The library covers a wide range in metallicity and contains most spectral types with an effective temperature range of 3100–50,000 K, gravity range of 0.0–5.0 dex, and metallicity range from −1.5 to +0.5 dex. The catalog contains 5584 spectra covering spectral types from O- to M-type and some special types such as A supergiant, blue horizontal-branch, and carbon stars. All of the spectra have absolutely calibrated fluxes at certain characteristic wavelengths corresponding to the optical passbands with accuracy better than 2.9% by comparing with PanSTARRS1 g-, r-, and i-band photometry. The survey contains 5342 spectra with spectral energy distribution effective temperature, surface gravity, and metallicity and 242 spectra with only the effective temperature and surface gravity. These parameters are consistent with the spectroscopic derived parameters of the same stars. Compared to current empirical libraries, ATLAS-A contains more cool giant stars. The catalog including derived parameters and the stellar spectra have been publicly released.

The catalog from Ji et al. (2023) was matched with the AllWISE catalog to pull in the WISE magnitudes. The stars in the range $7 < W2 < 12.5$ were selected to be in the sensitivity range of the SPHEREx spectra. From this list, sources were selected that satisfied the SPLICES isolation criterion that the nearest 2MASS neighbor must be more than $6''.2$ distant from the target. This resulted in a sample of 1,828 stars from the initial list of 5,584 sources, most of the sources being eliminated in the first magnitude cut. These sources have SEL_TYPE == ATLAS in the catalog.

4.6.2 LAMOST Standards

The Sloan Digital Sky Survey (SDSS) Apache Point Observatory Galactic Evolution Experiment (APOGEE) is a high resolution, near infrared (1.5 - 1.7 μm), spectroscopic survey of 100,000 luminous Milky Way red giant stars. The survey extension, APOGEE-2, is continuing observations on the SDSS 2.5 m telescope, and will also include a campaign in the southern hemisphere, providing 400,000 additional stars.

Ho et al. (2017) derived stellar attributes (Teff, log g, [Fe/H], and [α/H]) by using "The Cannon" (Ness et al., 2015) to transfer labels from a set of APOGEE stars where these parameters have been determined precisely. This yielded parameters for 454,180 LAMOST-observed stars, of which 195,859 are not already in SPLICES and satisfy the S/N and saturation criteria of $7 < W2 < 12$ and have no 2MASS neighbors closer than $6''.2$. These standards were placed in SPLICES and have SEL_TYPE == LAMOST.
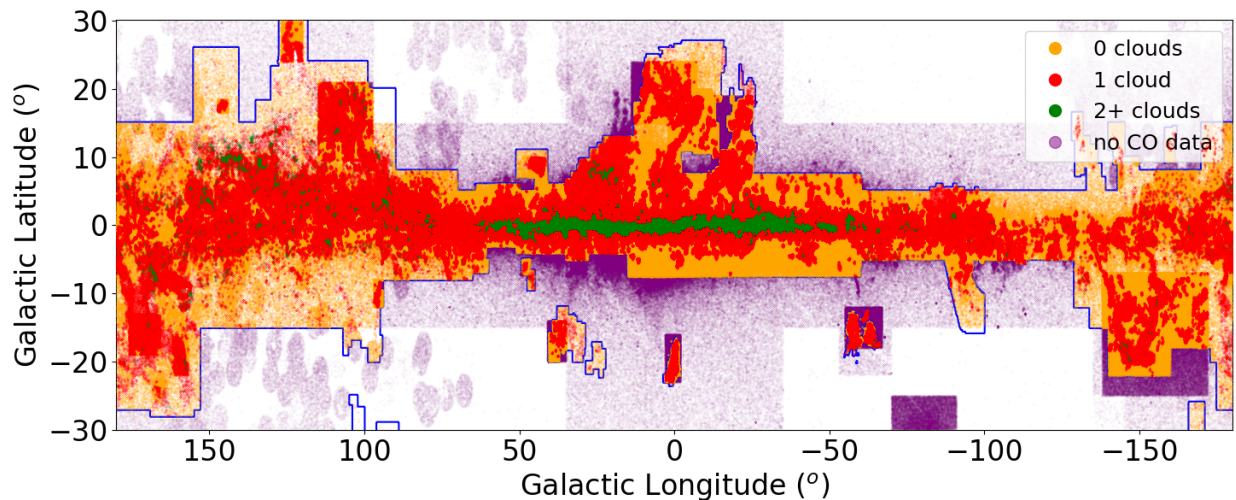

Figure 3: The number of CO clouds along each line of sight (NoC) values shown along the Galactic plane. The purple points are SPLICES version 8.6 targets, and the blue contours show the extent of the Dame et al. CO survey.

4.7 Number of Clouds Along the Line of Sight

One source of possible confusion to the SPHEREx Ices investigation is the case where the line of sight towards a source intercepts more than one cloud. In these cases, the absorption depth of the molecular features will represent the sum of the absorption depths within each cloud, and will mimic the case of a single cloud with the same total integrated absorption depth but higher peak absorption value in the cloud. This would affect the determination of the minimum optical depth necessary for ice formation in molecular clouds. For example, consider two sources where in one the line of sight passed through several low Av clouds that in total had the same Av as a different line of sight with a single higher density cloud. The single cloud could show ice absorption features while the line of sight through multiple clouds would not, even though they would have the same total Av to the background source. We therefore conducted an analysis to determine the number of clouds along each line of sight as measured by the CO survey by Dame et al. (2001).

The Dame et al. CO survey was conducted using 1.2 m telescopes with an 8 arcmin beam. The survey data were used to determine the number of CO clouds along each line of sight towards SPLICES targets.

The CO emission was examined toward each target sampled by the survey, and the number of CO peaks in velocity space above a certain threshold (corresponding to individual molecular clouds with different relative velocities in the emission line) were counted. The results are given in several columns in SPLICES. The `NoC` column gives the number of clouds along the line of sight value, with -1 for locations outside of the survey coverage. Also given for each target are `NoC_gl` and `NoC_gb` which are the Galactic longitude and latitude of the Dame et al. pixel. The results are shown in Figure 3. A total of $\sim 9.2 \times 10^6$ SPLICES targets are within the region surveyed in the Dame et al. survey.

Note that the `NoC` value represents clouds in the direction of the SPLICES target, but no estimate was made of the distances of the CO clouds or their relative positions with respect to the SPLICES target. Depending on the distance of the target, the source could be in front of all of the CO clouds, or behind one or more of the CO clouds detected.

4.8   Categorizing Intervening Clouds

An analysis was performed by SPHEREx Ices team member Miju Kang to determine the relationship between SPLICES targets and well-known nearby molecular clouds. The star formation handbook list from Zucker et al. (2020) was used, which provided foreground extinction and distance values for 326 sightlines in nearby star-forming regions.

Since many of the SPLICES sightlines point towards small cores or H II regions, it is essential to incorporate the dense structures surrounding them. The study by Spilker et al. (2021) provides cloud boundaries, including those for the sightlines from Zucker et al. (2020), to analyze a census of molecular clouds within 2 kpc of the Sun. They grouped together sightlines that are close to each other and have similar distances into single clouds. While their cloud boundaries were primarily used in this work, some adjustments were made to include the sightlines from Zucker et al. (2020) For regions like L379, IC2944, and Carina, which are beyond 2 kpc, the boundaries were determined based on the sightlines provided by Zucker et al. (2020).

Within each cloud, all SPLICES targets that fall within the projected 2D boundary on the sky are selected, totaling 3,122,371 targets. Within this subset, associations with the clouds are established based on whether the objects are in the foreground, within, or behind the cloud. This determination relies on two conditions: the Gaia distances of targets and the distance of the cloud, along with estimated Av of targets and the foreground Av to the cloud. Here, "cloud size" refers to half the major axis of the rectangle enclosing the cloud. The relationship of each source within the cloud boundary to the cloud itself is classified according to the following criteria, with the code appearing in the column `MC_Los` in SPLICES version 8.6:

- `FF`: The object is classified as foreground because its distance is less than the cloud distance minus the estimated cloud size, and the estimated Av is equal to or less than the foreground Av to the cloud.

- `IN`: The object is classified as within the cloud because its distance falls within ± 1 cloud size of the cloud distance, and the Av is greater than the foreground Av to the cloud.

- `BB`: The object is categorized as behind the cloud because its distance is greater than the distance to the cloud plus the cloud size, and the Av is greater than the foreground Av to the cloud.

- `FI`: The object is classified as foreground because its distance is less than the cloud distance minus the estimated cloud size. However, the estimated Av is greater than the foreground Av to the cloud, inconsistently.

- `BI`: The object is classified as inside or behind the cloud because its distance is greater than the cloud distance minus the cloud size. However, the estimated Av is equal to or less than the foreground Av to the cloud, inconsistently.

- `FE`: The object is classified in the foreground because the estimated Av is less than the foreground Av to the cloud, even though the object does not have a Gaia distance.

- `BE`: The object is classified as inside or in the background because the estimated Av is equal to or greater than the foreground Av to the cloud, even though the object does not have a Gaia distance.

Table 2: Cloud Catalog

Name	l_{lower} (deg)	l_{upper} (deg)	b_{lower} (deg)	b_{upper} (deg)	Dist. (pc)	Av (mag)	size (pc)	Number of Targets	Known YSOs
Aquila	12.0	35.0	6.0	18.0	237	0.6	109	154725	49
Aquila-South	28.8	40.5	-20.2	-12.2	132	0.1	33	19805	0
Ara	-25.0	-22.0	-3.5	-0.3	1055	0.9	81	59428	159
California	152.0	168.0	-11.0	-2.0	452	0.3	146	34907	83
Camelopardalis	140.6	155.1	14.6	25.9	281	0.1	90	5037	0
Carina	-74.2	-71.5	-1.5	0.6	2498	0.6	149	16942	286
CephFlare	97.0	116.5	5.1	25.0	595	0.2	295	122137	132
Chamaeleon	-70.0	-50.0	-22.0	-6.0	187	0.4	85	52325	131
Circinus	-48.0	-39.0	-8.0	-2.0	679	0.5	129	65973	3
CMaOB1	-138.0	-133.0	-3.5	1.8	1241	0.2	158	17607	499
Coalsack	-61.4	-55.7	-4.0	4.5	189	0.2	34	140757	540
Cygnus	73.0	87.0	-4.0	5.0	1013	0.7	296	300089	6281
CygOB7	89.1	95.5	1.5	6.5	604	0.7	86	52479	433
GemOB1	-172.0	-164.0	-4.0	2.1	1848	0.9	325	30097	690
GGD4	-178.5	-172.6	-6.5	-1.5	1356	0.6	183	9151	19
Hercules	41.0	49.0	6.0	11.0	225	0.1	37	22176	0
IC1396	97.5	102.5	0.5	5.1	918	0.7	109	31282	277
IC2944	-66.3	-64.7	-2.4	-1.1	2386	0.9	86	7402	106
IC443	-173.5	-168.5	2.5	7.5	1592	0.6	197	5112	0
IC5146	92.0	96.0	-7.0	-3.0	762	0.4	75	3146	86
L1265	115.5	119.0	-5.5	-1.6	344	0.4	31	5563	0
L1293-1306	119.0	128.0	-4.0	0.5	958	0.7	169	20262	64
L1307-35	123.2	131.4	0.8	6.5	794	1.0	139	32717	195
L1333	125.5	132.5	13.0	16.5	283	0.3	39	1165	1
L1340-55	128.4	135.4	7.0	12.6	910	0.8	143	8516	72
L291	10.3	14.1	-5.5	-1.5	1374	0.9	132	66731	49
L379	16.4	17.5	-3.3	-1.8	2119	0.9	69	7936	0
Lacerta	94.2	107.5	-20.1	-9.1	488	0.1	148	8524	1
Lagoon	6.0	8.0	-3.5	-1.0	1272	0.8	71	37604	109
LamOri	-170.0	-160.0	-18.0	-7.0	409	0.2	107	49786	170
LBN906-17	-159.0	-155.0	-32.6	-29.2	260	0.1	24	211	0
LBN968-CB28	-157.5	-150.5	-29.0	-21.2	332	0.2	61	6878	49
LBN991	-147.0	-145.0	-30.0	-28.0	408	0.2	20	64	0
Lupus	-28.0	-12.1	4.0	20.0	168	0.4	67	282667	168
M16	15.0	18.8	0.0	1.8	1627	1.2	119	55408	273
M17	13.5	16.0	-1.5	0.0	1524	0.8	78	28620	192
M20	6.0	8.0	-1.0	1.0	1214	0.7	60	33961	146
Maddalena	-146.0	-140.0	-5.0	1.0	2052	0.2	305	18153	257
MonOB1	-164.0	-153.0	-0.5	3.5	749	0.2	153	21690	538
MonocerosR2	-149.0	-136.0	-16.0	-6.0	856	0.3	247	52555	175
NGC2362	-123.2	-117.5	-7.5	-2.5	1283	0.2	170	6568	1
NGC6604	16.5	20.0	1.8	4.0	1403	1.1	101	44419	134
Norma	-22.0	-19.0	-0.3	3.5	721	0.8	61	70255	175
Ophiuchus	-12.0	11.0	8.0	26.0	139	0.3	73	200854	282
OrionA	-156.0	-141.0	-21.1	-17.0	436	0.2	119	22853	1940
OrionB	-160.0	-150.0	-17.0	-4.0	428	0.2	123	52887	447
Pegasus-East	100.0	107.0	-33.2	-25.2	274	0.1	51	222	0
Pegasus-West	87.4	96.0	-42.7	-29.2	251	0.1	71	13652	1
Perseus	152.0	162.0	-29.0	-12.0	282	0.2	98	14908	491
Pipe	-5.0	7.0	2.0	8.0	180	0.2	42	373708	105
Polaris	117.0	129.9	16.9	38.0	385	0.1	169	10621	0
RCrA	-2.0	4.0	-24.2	-16.2	156	0.2	27	18530	39
Rosette	-156.0	-150.0	-4.0	-0.5	1343	0.3	163	13421	370
S235	171.0	175.0	1.0	4.0	1664	0.9	145	6092	112
Serpens	25.0	33.0	1.0	6.0	487	1.0	80	190420	1083
Taurus	165.0	177.0	-21.0	-11.0	147	0.2	40	25560	290
UrsaMajor	138.9	158.9	32.9	42.2	360	0.1	141	17681	0
Vela	-98.0	-85.0	-4.0	5.0	1119	0.5	311	131533	1213
W3-W4-W5	132.5	138.4	-1.5	3.5	1858	1.0	251	21890	970

- UE: This object is classified as unclassified because it does not have Av data, although Gaia distance is available.

- UU: The object is classified as unclassified because it lacks both Av and Gaia distance data.

Among the targets enclosed within the cloud boundary, 55% are categorized as foreground (FF), inside (IN), and background (BB) sources, utilizing extinction and distance data. The distance to objects from 40% of the targets (FE, BE, UE, and UU) remains undetermined, while approximately 5% of the targets exhibit inconsistent Av or distance information (FI and BI). Approximately 262,000 targets have $H - W2 > 1.55$ (Av > 10 mag of extinction). About 90% of them are categorized as BE.

Other columns added are the Galactic coordinates of the molecular cloud sightline from Zucker et al. (2020) (MC_Lon and MC_Lat), the assumed distance to the cloud (MC_Dist), and the assumed foreground Av to the cloud (MC_AvF). A list of clouds included in the analysis and their parameters is given in Table 2.

4.9 Neighboring Source Analysis

The SPLICES targets were selected based on the criterion that they not have any 2MASS neighbors within $6\rlap{.}''2$. However, the limited sensitivity and spatial resolution of 2MASS allows faint background stars to fall within the $6\rlap{.}''2$ radius, undetected by 2MASS. An analysis was performed on several large surveys relevant to SPHEREx to quantify the possible effects of confusion by these objects. It was determined from simulations of SPHEREx photometry that sources closer than $7\rlap{.}''6$ could have an effect on the photometry of the targets, so the surveys were searched for sources within this distance of SPLICES targets in each survey. The surveys searched were the Gaia DR3 catalog, the Spitzer/IRAC catalog (primarily the GLIMPSE surveys (Churchwell et al., 2009) and other large surveys of star forming regions), the UKIDSS Galactic Plane survey (Lucas et al., 2008), and the VISTA Variables in the Vía Láctea (VVV) survey of the southern Galactic plane and bulge (Minniti et al., 2010).

Individual sources fainter than 17 mag Vega will be a factor of 100 below the faintest SPLICES sources at wavelengths >2.5 μm, but for highly extinced sources, they may contribute significant flux at optical or near-IR wavelengths. Also, if there are enough field sources close to the SPLICES target, their combined flux may affect the photometry. We have therefore found the number of field sources around SPLICES targets in these surveys, and summarized the results in several columns for each survey as summarized below.

4.9.1 Gaia DR3

The faintest Gaia sources detected can be fainter than G = 20 mag (Vega), therefore many SPHEREx targets will have field sources within $7\rlap{.}''6$. The Gaia catalog was searched around each SPLICES source and the magnitudes and positions of the nearest neighbors were found. The following information was calculated and placed in SPLICES columns:

- numGaiaNB - Number of Gaia sources <7.6 arcsec from target

- maxRmag - Maximum Gaia R mag of neighbors

- sumRflux - Sum of Gaia R band fluxes of neighbors

- mainRflux - SPLICES target Gaia R flux

- fluxratioGaia - Ratio of total background Gaia flux to SPLICES source flux

- minGaiaDist - Distance to nearest Gaia neighbor

- minDistGaiaFlux - Flux of nearest Gaia neighbor

Note that the Gaia magnitudes for SPLICES sources were already present in the GaiaDR3_G, GaiaDR3_B, GaiaDR3_R columns defined in earlier SPLICES versions.

4.9.2 IRAC

A similar search was performed for IRAC sources near SPLICES targets at 3.6 and 4.5 μm (IRAC bands I1 and I2). The sky coverage of the IRAC data is non-uniform, primarily consisting of ± 1 degree from the Galactic plane, although higher latitudes were surveyed in the bulge and some selected longitudes. The IRAC bands sample the wavelengths where ice absorption features are expected, so nearby sources could have a significant effect on the SPHEREx photometry. IRAC also has better spatial resolution ($\sim 2''$ compared to $4''$ for 2MASS and $6''$ for WISE), so it is able to find cases with close companions not rejected by the original SPLICES source selection. A set of columns similar to the Gaia columns were added to SPLICES, with separate values for the IRAC I1 and I2 bands. The column names are listed in Table 3. IRAC neighbors were found for $\sim 26\%$ of SPLICES targets. The coverage of the IRAC surveys is shown in Figure 4.
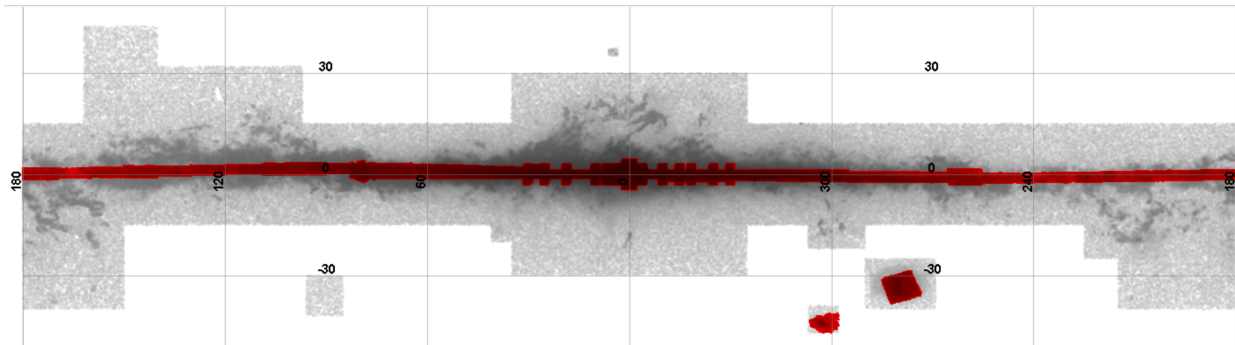

Figure 4: The sky coverage of the IRAC surveys (red points) used to check for neighbors to SPLICES targets. The SPLICES version 7.3 sources are shown in gray. The plot is in Galactic coordinates.

4.9.3 UKIDSS GPS

A similar search was performed in the $JHKs$ bands of the UKIDSS Galactic Plane Survey version DR6. A total of 18% of SPLICES targets had UKIDSS neighbors. Separate statistics were calculated for each band, and the column names are listed in Table 3. The UKIDSS catalog had many cases of spurious sources, so detections in more than one UKIDSS band was required before it was considered a valid source. The distribution of the sources checked is shown in Figure 5.
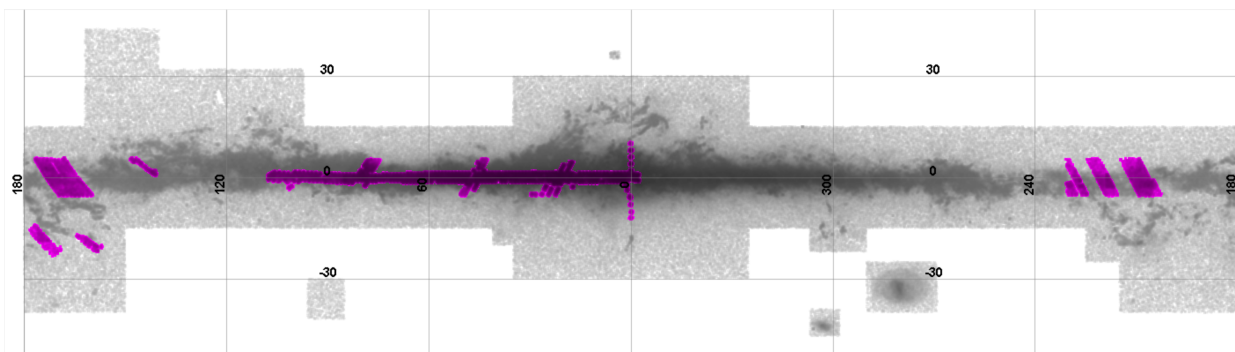
Figure 5: The sky coverage of the UKIDSS GPS (pink points) used to check for neighbors to SPLICES targets. The SPLICES version 7.3 sources are shown in gray. The plot is in Galactic coordinates.

4.9.4 VVV Survey

A similar search was performed in the $JHKs$ bands of the VVV Galactic Plane Survey version DR4.2. A total of 29% of SPLICES targets had VVV neighbors. Separate statistics were calculated for each band, and

Figure 6: The sky coverage of the VVV survey (green points) used to check for neighbors to SPLICES targets. The SPLICES version 7.3 sources are shown in gray. The plot is in Galactic coordinates.

the column names are listed in Table 3. The VVV catalog had many cases of spurious sources, so detections in more than one VVV band was required before it was considered a valid source. The distribution of the sources checked is shown in Figure 6.
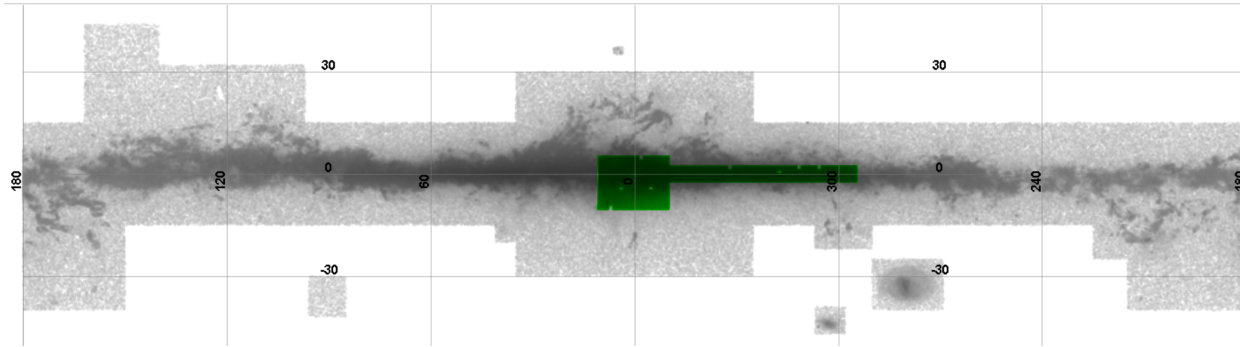
4.10 Gaia Variability

Eyer et al. (2023) provided a catalog of variable stars and other objects found in the Gaia DR3 database, along with a categorization of the type of object. We have added two columns to SPLICES: the `VarClassGaia` parameter which lists the best variability class determined by Eyer et al. (2023), and `VarClassGaiaSc` which is the "score" or estimate of the probability that the classification is correct (ranges from 0 - 1). Approximately 10% of SPLICES targets are identified as variable by Gaia.

4.11 NEOWISE Short-Term Variability

Ices team members Kyla Noh and Jeong-Eun Lee performed an analysis of the NEOWISE short-term variability of the SPLICES targets. They looked at the individual WISE photometric measurements of sources which consist of ∼20 exposures measured over 1-2 days, with a cadence of 6 months. Sources with magnitude uncertainties of < 0.2 were examined, and the number of epochs where the standard deviation of the flux measurements was greater than $3\times$ the photometric uncertainty were counted. A variability flag was determined for each source examined in each WISE band (columns `SV_W1` and `SV_W2` in SPLICES), where "N" means no short-term variability was detected, "V" means the variability criterion was met in one or more epochs, and "U" means that there were no epochs where the photometric uncertainty was < 0.2 mag. Also given for each band are the number of variable epochs (`SV_W1_V` and `SV_W2_V`) and the total number of epochs examined (`SV_W1_T` and `SV_W2_T`).

5   SPLICES Column Definitions

Table 3 lists the SPLICES column definitions for the current version. See Ashby et al. (2023) and the above sections for more details on the various entries.

The units are specified where applicable. deg = degrees, mag - magnitudes in the Vega system, arcsec = arcseconds, mas.yr**-1 = milli-arcseconds per year, pc = parsec, μJy = micro-Janskys.

Table 3: SPLICES Columns

Parameter	Description	Units
source_id	SPLICES source ID	
designation	Source Designation	
ra	Right ascension (J2000.0)	deg
dec	Declination (J2000.0)	deg
GAL_LONG	Galactic Longitude	deg
GAL_LAT	Galactic Latitude	deg
tmassdesignation	2MASS source designation	
tmassra	2MASS right ascension (J2000.0)	deg
tmassdec	2MASS declination (J2000.0)	deg
J	2MASS J magnitude	mag
Jerr	2MASS J magnitude uncertainty	mag
H	2MASS H magnitude	mag
Herr	2MASS H magnitude uncertainty	mag
K	2MASS K magnitude	mag
Kerr	2MASS K magnitude uncertainty	mag
ph_qual	2MASS photometric quality flags	
rd_flg	2MASS rd_flg flag	
prox	2MASS prox value	arcsec
W1	WISE band 1 magnitude	mag
W1err	WISE band 1 magnitude uncertainty	mag
W2	WISE band 2 magnitude	mag
W2err	WISE band 2 magnitude uncertainty	mag
W3	WISE band 3 magnitude	mag
W3err	WISE band 2 magnitude uncertainty	mag
W4	WISE band 4 magnitude	mag
W4err	WISE band 2 magnitude uncertainty	mag
cc_flags	WISE cc_flags	
ext_flg	WISE ext_flg flag	
var_flg	WISE var_flg flag	
IRAC_designation	IRAC source designation	
ra_IRAC	IRAC right ascension (J2000.0)	deg
dec_IRAC	IRAC declination (J2000.0)	deg
mag3_6	IRAC 3.6 micron magnitude	mag
d3_6m	IRAC 3.6 micron magnitude uncertainty	mag
mag4_5	IRAC 4.5 micron magnitude	mag
d4_5m	IRAC 4.5 micron magnitude uncertainty	mag
mag5_8	IRAC 5.8 micron magnitude	mag
d5_8m	IRAC 5.8 micron magnitude uncertainty	mag
mag8_0	IRAC 8.0 micron magnitude	mag
d8_0m	IRAC 8.0 micron magnitude uncertainty	mag
SEL_TYPE	Source selection method	
CLASS_1	Source Class	
YSO_PUB	Publication source of YSO classification	
	Continued on next page	

Table 3 – continued from previous page

Parameter	Description	Units
STYPE_ML	Machine Learning Source Class	
STYPE_ML_PROB1	Machine Learning Source Type Probability Stage 1	
STYPE_ML_PROB2	Machine Learning Source Type Probability Stage 2	
NAME	Proper Name	
Gaia_DR3	Gaia DR3 source designation	
GaiaDR3_G	Gaia G band magnitude	mag
GaiaDR3_Gerr	Gaia G band magnitude uncertainty	mag
GaiaDR3_B	Gaia B band magnitude	mag
GaiaDR3_Berr	Gaia B band magnitude uncertainty	mag
GaiaDR3_R	Gaia R band magnitudeD	mag
GaiaDR3_Rerr	Gaia R band magnitude uncertainty	mag
Plx	Gaia parallax	mas
e_Plx	Gaia parallax uncertainty	mas
pmra	Right Ascension proper motion	mas.yr**-1
pmra_err	Right Ascension proper motion uncertainty	mas.yr**-1
pmdec	Declination proper motion	mas.yr**-1
pmdec_err	Declination proper motion uncertainty	mas.yr**-1
Dist	Distance derived by Gaia	pc
e_Dist_upper	Upper limit of distance 68% confidence range	pc
e_Dist_lower	Lower limit of distance 68% confidence range	pc
CLASSvar	Source Class from variability analysis	
W1var	W1 variability flag	
W1var_CLASS	W1 variability class	
W2var	W2 variability flag	
W2var_CLASS	W2 variability class	
W1VARAVG	NEOWISE W1 mean mag	mag
W2VARAVG	NEOWISE W2 mean mag	mag
W1VARAMP	NEOWISE W1 variability amplitude	mag
W2VARAMP	NEOWISE W2 variability amplitude	mag
Av	Estimate of Av from H-W2 or K-W2	mag
MC	Molecular Cloud name	
MC_Lon	Galactic longitude of cloud sightline	deg
MC_Lat	Galactic latitude of cloud sightline	deg
MC_Dist	Distance of cloud	pc
MC_AvF	Foreground Av to cloud	mag
MC_Los	Position class	
numGaiaNB	Number of Gaia sources <7.6 arcsec from target	
maxRmag	Maximum Gaia R mag of neighbors	mag
sumRflux	Sum of Gaia R band fluxes of neighbors	uJy
mainRflux	SPLICES target Gaia R flux	uJy
fluxratioGaia	Ratio of bkgnd Gaia flux to SPLICES source flux	percent
minGaiaDist	Distance to nearest Gaia neighbor	arcsec
minDistGaiaFlux	Flux of nearest Gaia neighbor	uJy
NoC	Number of clouds along the line of sight (Dame et al.)	
NoC_gl	Galactic longitude of Dame et al. pixel	deg
NoC_gb	Galactic latitude of Dame et al. pixel	deg
numIRACnbors	Number of IRAC sources <7.6 arcsec from target	
minDistIRAC	Distance of closest neighbor	arcsec
I1mag	I1 mag of SPLICES target	mag
maxI1mag	I1 mag of brightest neighbor	mag
sumI1flux	Sum of I1 neighbor fluxes	uJy
	Continued on next page	

Table 3 – continued from previous page

Parameter	Description	Units
mainI1flux	I1 Flux of SPLICES target	uJy
minDistI1flux	I1 Flux of closest neighbor	uJy
I2mag	I2 mag of SPLICES target	mag
maxI2mag	I2 mag of brightest neighbor	mag
sumI2flux	Sum of I1 neighbor fluxes	uJy
mainI2flux	I2 Flux of SPLICES target	uJy
minDistI2flux	I2 Flux of closest neighbor	uJy
fluxratioI1	Ratio of bkgnd I1 flux to SPLICES source flux	percent
fluxratioI2	Ratio of bkgnd I2 flux to SPLICES source flux	percent
numVVVneighbors	Number of VVV sources <7.6 arcsec from target	
minDistVVV	Distance to nearest VVV neighbor	arcsec
VVVJmag	VVVJ mag of SPLICES target	mag
maxVVVJmag	VVVJ mag of brightest nearby source	mag
sumVVVJflux	Sum of VVVJ fluxes of background sources	uJy
mainVVVJflux	J band Flux of SPLICES source	uJy
minDistVVVJFlux	Flux of nearest VVVJ background source	uJy
VVVHmag	VVVH mag of SPLICES target	mag
maxVVVHmag	VVVH mag of brightest nearby source	mag
sumVVVHflux	Sum of VVVH fluxes of background sources	uJy
mainVVVHflux	H band Flux of SPLICES source	uJy
minDistVVVHFlux	Flux of nearest VVVH background source	uJy
VVVKmag	VVVK band mag of SPLICES source	mag
maxVVVKmag	VVVK mag of brightest nearby source	mag
sumVVVKflux	Sum of VVVK fluxes of background sources	uJy
mainVVVKflux	K band Flux of SPLICES source	uJy
minDistVVVKFlux	Flux of nearest VVVK background source	uJy
fluxratioVVVJ	Ratio of bkgnd VVVJ flux to SPLICES source flux	percent
fluxratioVVVH	Ratio of bkgnd VVVH flux to SPLICES source flux	percent
fluxratioVVVK	Ratio of bkgnd VVVK flux to SPLICES source flux	percent
numUKSnbors	Number of UKIDSS sources <7.6 arcsec from target	
minDistUKS	Distance to closest UKIDSS neighbor	arcsec
UKSJmag	UKSJ band mag of SPLICES source	mag
maxUKSJmag	UKSJ mag of brightest nearby source	mag
sumUKSJflux	Sum of UKSJ fluxes of background sources	uJy
mainUKSJflux	J band Flux of SPLICES source	uJy
minDistUKSJFlux	Flux of nearest UKSJ background source	uJy
UKSHmag	UKSH band mag of SPLICES source	mag
maxUKSHmag	UKSH mag of brightest nearby source	mag
sumUKSHflux	Sum of UKSH fluxes of background sources	uJy
mainUKSHflux	H band Flux of SPLICES source	uJy
minDistUKSHFlux	Flux of nearest UKSH background source	uJy
UKSKmag	UKSK band mag of SPLICES source	mag
maxUKSKmag	UKSK mag of brightest nearby source	mag
sumUKSKflux	Sum of UKSK fluxes of background sources	uJy
mainUKSKflux	K band Flux of SPLICES source	uJy
minDistUKSKFlux	Flux of nearest UKSK background source	uJy
fluxratioUKSJ	Ratio of bkgnd UKSJ flux to SPLICES source flux	percent
fluxratioUKSH	Ratio of bkgnd UKSH flux to SPLICES source flux	percent
fluxratioUKSK	Ratio of bkgnd UKSK flux to SPLICES source flux	percent
VarClassGaia	Gaia Variability best class	
VarClassGaiaSc	Score of the best Gaia class	

Table 3 – continued from previous page

Parameter	Description	Units
SV_W1	NEOWISE W1 short-term variability flag	
SV_W1_V	Number of W1 variable short-term epoch	
SV_W1_T	Number of W1 total short-term epochs	
SV_W2	NEOWISE W2 short-term variability flag	
SV_W2_V	Number of W2 variable short-term epochs	
SV_W2_T	Number of W2 total short-term epochs	

References

Ashby, M. L. N., Hora, J. L., Lakshmipathaiah, K., et al. 2023, ApJ, 949, 105, doi: `10.3847/1538-4357/acc86b`

Chen, C. H., Mittal, T., Kuchner, M., et al. 2014, ApJS, 211, 25, doi: `10.1088/0067-0049/211/2/25`

Churchwell, E., Babler, B. L., Meade, M. R., et al. 2009, PASP, 121, 213, doi: `10.1086/597811`

Cui, X.-Q., Zhao, Y.-H., Chu, Y.-Q., et al. 2012, Research in Astronomy and Astrophysics, 12, 1197, doi: `10.1088/1674-4527/12/9/003`

Dame, T. M., Hartmann, D., & Thaddeus, P. 2001, ApJ, 547, 792, doi: `10.1086/318388`

Eyer, L., Audard, M., Holl, B., et al. 2023, A&A, 674, A13, doi: `10.1051/0004-6361/202244242`

Ho, A. Y. Q., Ness, M. K., Hogg, D. W., et al. 2017, ApJ, 836, 5, doi: `10.3847/1538-4357/836/1/5`

Ji, W., Liu, C., Deng, L., et al. 2023, ApJS, 265, 61, doi: `10.3847/1538-4365/acbf42`

Lakshmipathaiah, K., Vig, S., Ashby, M. L. N., et al. 2023, MNRAS, 526, 1923, doi: `10.1093/mnras/stad2782`

Lucas, P. W., Hoare, M. G., Longmore, A., et al. 2008, MNRAS, 391, 136, doi: `10.1111/j.1365-2966.2008.13924.x`

Majewski, S. R., Zasowski, G., & Nidever, D. L. 2011, ApJ, 739, 25, doi: `10.1088/0004-637X/739/1/25`

Minniti, D., Lucas, P. W., Emerson, J. P., et al. 2010, NewA, 15, 433, doi: `10.1016/j.newast.2009.12.002`

Mittal, T., Chen, C. H., Jang-Condell, H., et al. 2015, ApJ, 798, 87, doi: `10.1088/0004-637X/798/2/87`

Ness, M., Hogg, D. W., Rix, H. W., Ho, A. Y. Q., & Zasowski, G. 2015, ApJ, 808, 16, doi: `10.1088/0004-637X/808/1/16`

Patel, R. I., Metchev, S. A., & Heinze, A. 2014, ApJS, 212, 10, doi: `10.1088/0067-0049/212/1/10`

Patel, R. I., Metchev, S. A., Heinze, A., & Trollo, J. 2017, AJ, 153, 54, doi: `10.3847/1538-3881/153/2/54`

Spilker, A., Kainulainen, J., & Orkisz, J. 2021, A&A, 653, A63, doi: `10.1051/0004-6361/202040021`

Zucker, C., Speagle, J. S., Schlafly, E. F., et al. 2020, A&A, 633, A51, doi: `10.1051/0004-6361/201936145`